JCI insight

RESEARCH ARTICLE

FGF21 underlies a hormetic response to metabolic stress in methylmalonic acidemia

Irini Manoli,[1] Justin R. Sysol,[1] Madeline W. Epping,[1] Lina Li,[1] Cindy Wang,[1] Jennifer L. Sloan,[1] Alexandra Pass,[1] Jack Gagné,[1] Yiouli P. Ktena,[1] Lingli Li,[2] Niraj S. Trivedi,[3] Bazoumana Ouattara,[4,5] Patricia M. Zerfas,[6] Victoria Hoffmann,[6] Mones Abu-Asab,[7] Maria G. Tsokos,[7] David E. Kleiner,[8] Caterina Garone,[9] Kristina Cusmano-Ozog,[10] Gregory M. Enns,[10] Hilary J. Vernon,[11] Hans C. Andersson,[12] Stephanie Grunewald,[13] Abdel G. Elkahloun,[3] Christiane L. Girard,[4] Jurgen Schnermann,[2] Salvatore DiMauro,[9] Eva Andres-Mateos,[14,15] Luk H. Vandenberghe,[14,15,16,17] Randy J. Chandler,[1] and Charles P. Venditti[1]

[1]Medical Genomics and Metabolic Genetics Branch, National Human Genome Research Institute, NIH, Bethesda, Maryland, USA. [2]Kidney Disease Branch, National Institute of Diabetes and Digestive and Kidney Diseases, NIH, Bethesda, Maryland, USA. [3]Genome Technology Branch, National Human Genome Research Institute, NIH, Bethesda, Maryland, USA. [4]Sherbrooke Research and Development Centre, Agriculture and Agri-Food Canada, Sherbrooke, Quebec, Canada. [5]Péléforo Gbon Coulibaly University, Korhogo, Ivory Coast. [6]Office of Research Services, NIH, Bethesda, Maryland, USA. [7]Ultrastructural Pathology Section, Center for Cancer Research, NIH, Bethesda, Maryland, USA. [8]Laboratory of Pathology, National Cancer Institute, NIH, Bethesda, Maryland, USA. [9]Department of Neurology, Columbia University Medical Center, New York, New York, USA. [10]Division of Medical Genetics, Stanford University, Stanford, California, USA. [11]McKusick-Nathans Institute of Genetic Medicine, Johns Hopkins University, Baltimore, Maryland, USA. [12]Hayward Genetics Center, Tulane University Medical School, New Orleans, Louisiana, USA. [13]Department of Pediatric Metabolic Medicine, Great Ormond Street Hospital for Children Foundation Trust, Institute of Child Health, UCL, London, United Kingdom. [14]Grousbeck Gene Therapy Center, Schepens Eye Research Institute and Massachusetts Eye and Ear Infirmary, Boston, Massachusetts, USA. [15]Ocular Genomics Institute, Department of Ophthalmology, Harvard Medical School, Boston, Massachusetts, USA. [16]Harvard Stem Cell Institute, Harvard University, Cambridge, Massachusetts, USA. [17]Broad Institute of Harvard and MIT, Cambridge, Massachusetts, USA.

Methylmalonic acidemia (MMA), an organic acidemia characterized by metabolic instability and multiorgan complications, is most frequently caused by mutations in methylmalonyl-CoA mutase (*MUT*). To define the metabolic adaptations in MMA in acute and chronic settings, we studied a mouse model generated by transgenic expression of Mut in the muscle. *Mut*$^{-/-}$;Tg$^{INS\text{-}MCK\text{-}Mut}$ mice accurately replicate the hepatorenal mitochondriopathy and growth failure seen in severely affected patients and were used to characterize the response to fasting. The hepatic transcriptome in MMA mice was characterized by the chronic activation of stress-related pathways and an aberrant fasting response when compared with controls. A key metabolic regulator, Fgf21, emerged as a significantly dysregulated transcript in mice and was subsequently studied in a large patient cohort. The concentration of plasma FGF21 in MMA patients correlated with disease subtype, growth indices, and markers of mitochondrial dysfunction but was not affected by renal disease. Restoration of liver *Mut* activity, by transgenesis and liver-directed gene therapy in mice or liver transplantation in patients, drastically reduced plasma FGF21 and was associated with improved outcomes. Our studies identify mitocellular hormesis as a hepatic adaptation to metabolic stress in MMA and define FGF21 as a highly predictive disease biomarker.

Authorship note: IM and JRS contributed equally to this work.

Conflict of interest: IM, RJC, and CPV are inventors on patents (12/418,795; 61/792,081; 62/556,071; 62/579,247) related to MMA filed by the NIH on their behalf. Lina Li is an employee of LLN Consultant Inc. and founder of CELiD Biotechnologies Inc. GME is a consultant for Moderna Therapeutics, LogicBio Therapeutics, Horizon Pharma, and Natera; a data-monitoring committee member for BioMarin, Audentes Therapeutics, Amicus, RegenxBio, and NeuroVia; and an investigator on clinical trials for Aeglea, BioElectron, and Stealth Therapeutics. LHV is an inventor of AncAAV and other AAV technologies, which are licensed to various biotechnology and pharmaceutical entities. LHV is a consultant to a number of companies with gene therapy interest, including Selecta Biosciences and Lonza, licensees of AncAAV technology. CPV has received funding to support AAV gene therapy research for MMA from Selecta Biosciences and LogicBio Therapeutics.

Submitted: August 22, 2018
Accepted: October 24, 2018
Published: December 6, 2018

Reference information:
JCI Insight. 2018;3(23):e124351. https://doi.org/10.1172/jci.insight.124351.

Introduction

In vertebrates, essential nutrients, including valine, isoleucine, methionine, and threonine, as well as odd-chain fatty acids and cholesterol, are oxidized to propionyl-CoA and subsequently metabolized to methylmalonyl-CoA in the mitochondrial matrix (1, 2). The terminal conversion of methylmalonyl-CoA to succinyl-CoA, a Krebs cycle intermediate, is mediated by the adenosylcobalamin-dependent methylmalonyl-CoA mutase (MUT)

(3–5). *MUT* is ubiquitously expressed and relatively abundant in the liver and kidney as well as the brain and skeletal muscle (6). MUT deficiency causes a life-threatening organic acidemia, termed methylmalonic acidemia (MMA) (7–11). Organic acidemias, along with maple syrup urine disease and urea cycle defects, are classified as "intoxication"-type inborn errors of metabolism. Patients with these disorders display a propensity to acute, and sometimes fatal, metabolic crises, which can be precipitated by intercurrent infections, dietary imbalance, fasting, or other stressful stimuli.

The treatment of MMA entails adherence to a low-protein diet, carnitine supplementation, and vigilant clinical monitoring (12–15) but cannot effectively prevent the acute or chronic complications of the disease (11, 16). The recalcitrant nature of MMA to conventional management has led to the implementation of elective liver or liver/kidney transplantation (LT or LKT) as a surgical treatment option for many patients (12, 17–21). Despite the continued metabolite production in extrahepatic tissues, such as the skeletal muscle (22–24), a successful LT or LKT confers remarkable metabolic stability upon the recipient, demonstrating the critical contribution of hepatic metabolism to the clinical phenotype of MMA.

While several studies have alluded to the complexity of disease mechanisms involved in MMA pathogenesis, the most compelling observations have demonstrated that a cell-specific, conditionally autonomous mitochondriopathy and associated electron transport chain defect(s) underlie the organ pathology seen in mice and patients (25–29). However, there is limited understanding of how a block in an essential oxidative pathway alters mitochondrial and cellular adaptation to stress and whether signaling molecules and pathways can be monitored to predict or evoke therapeutic responses.

Given the central role of the liver in MMA pathophysiology, we generated a viable mouse model to study the acute and chronic hepatic disease manifestations. Through transgenesis, we used the murine muscle creatine kinase (MCK) promoter to drive *Mut* expression in the skeletal muscle of the $Mut^{-/-}$ mice (23, 30). The resulting $Mut^{-/-}$;$Tg^{INS\text{-}MCK\text{-}Mut}$ animals were rescued from the neonatal lethality observed in $Mut^{-/-}$ mice but manifested the clinical and biochemical features of MMA, including severe growth retardation, fragility, massively elevated serum methylmalonic acid concentrations, and hepatorenal mitochondrial pathology. To recapitulate the acute-on-chronic metabolic crises intermittently experienced by MMA patients, we subjected these mice to a fasting challenge and explored changes in the hepatic transcriptome between the baseline and fasting states. Among the many pathways differentially expressed between MMA mice and control littermates, a key metabolic regulator, *Fgf21*, emerged as most significant. Moreover, a number of fasting-regulated genes, including *Fgf21*, were significantly upregulated in the $Mut^{-/-}$;$Tg^{INS\text{-}MCK\text{-}Mut}$ mice at baseline, suggesting that there is a chronic cellular/mitochondrial stress state that accompanies MMA. FGF21 elevations were validated in a large MMA patient cohort and shown to correlate with disease severity. We then used plasma Fgf21 to follow the effects of liver correction by transgenesis or hepatic gene addition in the mice and orthotopic LT in the patients. In aggregate, our results suggest that mitocellular hormesis, an adaptive response to the cellular dysfunction caused by the inborn error of metabolism, underlies the eventual failure of acute-on-chronic stress response in MMA and that the FGF21 axis appears to be a key marker, and likely mediator, of this response.

Results

Expression of Mut in skeletal muscle augments metabolism and rescues $Mut^{-/-}$ mice from neonatal lethality. Skeletal muscle constitutes 40% of the total body weight and is the site of a large fraction of whole-body branched-chain amino acid (BCAA) oxidation (22–24). Given the critical role of MUT in the terminal oxidation of BCAA, and the fact that skeletal muscle contains a relatively large amount of Mut activity in mice (31), we reasoned that targeted, permanent expression in this tissue might rescue $Mut^{-/-}$ mice from lethality. We designed a transgene to express the murine *Mut* complementary DNA under the control of an insulated murine MCK promoter (32), generated C57BL/6 $Tg^{INS\text{-}MCK\text{-}Mut}$ founder lines, and bred the transgene onto the enriched C57BL/6 $Mut^{-/-}$ background (Supplemental Figure 1A; supplemental material available online with this article; https://doi.org/10.1172/jci.insight.124351DS1). $Mut^{-/-}$;$Tg^{INS\text{-}MCK\text{-}Mut}$ mice were born in Mendelian proportions and were rescued from neonatal lethality, with 87% surviving to day of life 120 (Figure 1A). As expected, messenger RNA and immunoreactive Mut protein showed transgene overexpression that was limited to the skeletal and cardiac muscles (Supplemental Figure 1, B and C).

To further assess the in vivo enzymatic activity conferred by the muscle-limited transgene expression, we measured Mut activity directly in tissue extracts (33) and at the level of the whole body using a [1-^{13}C] sodium propionate oxidation breath testing method, as described previously (27, 34). Compared with wild-type

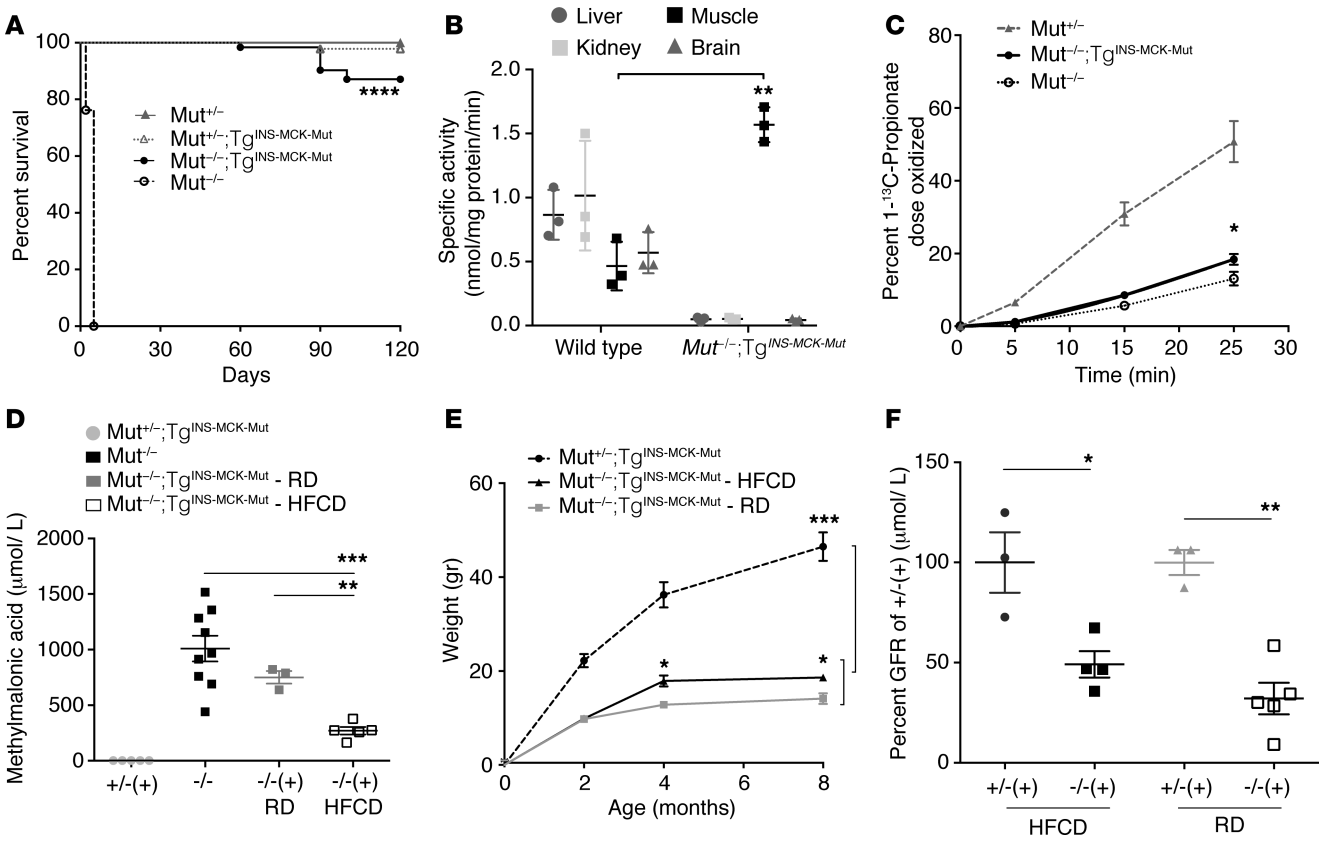

Figure 1. Phenotypic characterization of the muscle transgenic MMA mouse model. (**A**) *Mut*$^{-/-}$;Tg$^{INS\text{-}MCK\text{-}Mut}$ mice (n = 62) exhibit near normal survival compared with the neonatal lethality of *Mut*$^{-/-}$ mice (n = 42; log-rank Mantel-Cox and Gehan-Breslow-Wilcoxon test, $P < 0.0001$) and comparable to their heterozygote littermates (n = 46 and 28, respectively; P = NS). (**B**) Mut-specific activity was undetectable in the liver, kidney, and brain extracts of *Mut*$^{-/-}$;Tg$^{INS\text{-}MCK\text{-}Mut}$ mice, while it was approximately 3 times higher in skeletal muscle compared with that in wild-type controls (1.57 ± 0.07 vs. 0.46 ± 0.11nmol/mg protein/min, n = 3, P = 0.001, unpaired t test). (**C**) [1-^{13}C] propionate in vivo oxidation showed a small but significant increase by the muscle transgene-mediated *Mut* expression (n = 3, 6, and 4 for *Mut*$^{+/-}$, *Mut*$^{-/-}$;Tg$^{INS\text{-}MCK\text{-}Mut}$, and *Mut*$^{-/-}$, respectively; P = 0.04 between mice with and without the transgene). (**D**) Plasma methylmalonic acid concentrations in *Mut*$^{-/-}$;Tg$^{INS\text{-}MCK\text{-}Mut}$ mice were lower compared with *Mut*$^{-/-}$ mice when animals were reared on high-fat and carbohydrate (HFCD) but not on regular chow diet (RD) (P = 0.0006, n = 3–5, 1-way ANOVA with Tukey's test for multiple comparisons). (**E**) Somatic growth was impaired, with *Mut*$^{-/-}$;Tg$^{INS\text{-}MCK\text{-}Mut}$ mice not exceeding 50% of the weight of their littermates throughout their life span (P = 0.0002). High caloric diet resulted in improved weight compared with regular chow (P = 0.022, n = 7 mice per group). (**F**) Glomerular filtration rate (GFR) in *Mut*$^{-/-}$;Tg$^{INS\text{-}MCK\text{-}Mut}$ mice was 49.15% ± 6.6% of the average GFR in heterozygote mice on HFCD and 32.1 ± 7.89% on RD (n = 3 and 5, P = 0.05 on HFCD and n = 3 and 4, P = 0.035 for RD, Mann-Whitney U test). GFR between the different diets was not significant. Values are mean ± SEM. *$P < 0.05$, **$P < 0.01$, ***$P < 0.001$, ****$P < 0.0001$).

controls, *Mut*$^{-/-}$;Tg$^{INS\text{-}MCK\text{-}Mut}$ mice had absent/trace enzyme activity in the liver, kidney, and brain but approximately 3 times higher activity in extracts prepared from skeletal muscle (Figure 1B and Supplemental Methods). The oxidation of [1-^{13}C] sodium propionate into $^{13}CO_2$ showed that *Mut*$^{-/-}$;Tg$^{INS\text{-}MCK\text{-}Mut}$ mice metabolized 18.4% ± 3.6% of the [1-^{13}C] propionate isotopomer in 25 minutes, compared with 50.7% ± 9.8% in *Mut*$^{+/-}$ animal s and 13.1 ± 3.8% in *Mut*$^{-/-}$ animals (Figure 1C and Supplemental Methods). To facilitate a comparison between the *Mut*$^{-/-}$;Tg$^{INS\text{-}MCK\text{-}Mut}$ mice and those from a liver transgenic MMA model (*Mut*$^{-/-}$;Tg$^{INS\text{-}Alb\text{-}Mut}$) described previously (27), we expressed propionate oxidation as the percentage of heterozygote control levels. We observed a significantly lower propionate oxidative capacity in the muscle transgenic *Mut*$^{-/-}$;Tg$^{INS\text{-}MCK\text{-}Mut}$ mice (36.2% ± 7.1% control) compared with the liver transgenic *Mut*$^{+/-}$;Tg$^{INS\text{-}Alb\text{-}Mut}$ mice (78.04% ± 22.1%) (Supplemental Figure 1D). Although the liver transgenic mice only expressed 8.2% ± 1% of wild-type *Mut* mRNA, as opposed to 19,492.5% ± 6,623.5% measured in the *Mut*$^{-/-}$;Tg$^{INS\text{-}MCK\text{-}Mut}$ mice compared with their *Mut*$^{+/+}$ littermates (Supplemental Figure 1B), the effects on the disease phenotype were pronounced between liver versus muscle correction.

The increased Mut enzyme activity in the skeletal muscle resulted in a sustained reduction of plasma methylmalonic acid concentrations compared with historical values from *Mut*$^{-/-}$ mice (1,009 ± 348.6 µmol/l). Average methylmalonic acid concentrations in *Mut*$^{-/-}$;*Tg*$^{INS\text{-}MCK\text{-}Mut}$ mice were 750.3 ± 98 µmol/l

when reared on regular chow (RD) and 269.5 ± 75.8 μmol/l on high-fat and carbohydrate (HFCD) diets (Figure 1D). *Mut*$^{-/-}$;*Tg*$^{INS\text{-}MCK\text{-}Mut}$ mice fed a high-fat diet had methylmalonic acid levels 35% of those reared on RD, as expected, given the higher protein content in the RD diet.

Mut$^{-/-}$;*Tg*$^{INS\text{-}MCK\text{-}Mut}$ *mice manifest severe growth failure, are resistant to obesity, and exhibit hepatorenal mitochondrial pathology similar to MMA patients*. Similar to the severe growth failure typically observed in MMA patients (13, 35), *Mut*$^{-/-}$;Tg$^{INS\text{-}MCK\text{-}Mut}$ mice remained smaller than *Mut*$^{+/-}$;Tg$^{INS\text{-}MCK\text{-}Mut}$ littermates throughout their life span (Figure 1E and Supplemental Figure 1E). These mice required nutritional supplementation with high-fat chow and carbohydrates to survive, a diet resembling that used for the management of MMA patients (13, 35). While *Mut*$^{-/-}$;Tg$^{INS\text{-}MCK\text{-}Mut}$ mice only achieved 25%–30% of their heterozygous littermates weights when fed RD, they were able to achieve 40%–50% of *Mut*$^{+/-}$;Tg$^{INS\text{-}MCK\text{-}Mut}$ mouse weight on the HFCD. Both diets were ingested based on observations from stool production and intestinal contents at necropsy. Heterozygote and wild-type littermates uniformly became obese on the same diet (Figure 1E).

Given that chronic kidney disease develops in over 60% of the severe *mut*^{0} MMA patients in the first decade of life (termed *mut*^{0} for the lack of residual enzyme activity and response of propionate incorporation to hydroxocobalamin in fibroblast studies, as compared with *mut*$^{-}$ for partial enzyme deficiency) (16), we measured glomerular filtration rate (GFR) using FITC-inulin clearance in *Mut*$^{-/-}$;*Tg*$^{INS\text{-}MCK\text{-}Mut}$ mice, as was previously described in the liver transgenic mouse model (*Mut*$^{-/-}$;*Tg*$^{INS\text{-}Alb\text{-}Mut}$) (27). *Mut*$^{-/-}$;*Tg*$^{INS\text{-}MCK\text{-}Mut}$ mice indeed had impaired renal function, with a 49% filtration rate compared with heterozygote littermates on HFCD, which was more impaired at 32% on RD (Figure 1F and Supplemental Methods).

The *Mut*$^{-/-}$;Tg$^{INS\text{-}MCK\text{-}Mut}$ animals developed liver pathology, characterized by prominent bright Mallory bodies in the cytoplasm, as well as numerous paler eosinophilic vacuoles that often fill the cytoplasm, consistent with megamitochondria (Supplemental Figure 2A, b and c, in comparison to heterozygote littermates, Supplemental Figure 2Aa). Furthermore, electron microscopy of *Mut*$^{-/-}$;*Tg*$^{INS\text{-}MCK\text{-}Mut}$ livers showed mitochondria that were enlarged with shortened or no cristae (Figure 2A, middle and right compared with heterozygote controls on the left). These findings were associated with decreased respiratory chain complex IV staining and activity (Supplemental Figure 3, A and B) and reduced oxidation rates of [1-^{13}C] labeled substrates that depend on mitochondrial function for their metabolism, including [1-^{13}C] methionine and [1-^{13}C] glycine (Supplemental Figure 3, C and D).

We sought to compare the pathological findings in the mice to those observed in MMA patients who underwent an orthotopic liver or a combined LKT. Histology and electron microscopy were used to characterize pathological changes (Supplemental Figure 2B, a–c and d–i, respectively). Findings in the human samples closely resembled that noted in the mice. The MMA patient livers displayed primarily macrovesicular periportal steatosis. Nuclear vacuolation/glycogenation was observed in periportal hepatocytes, a finding resembling nonalcoholic fatty liver disease. Patchy areas of pale, glycogen-rich hepatocytes, some with a ground-glass appearance, distributed in a nonzonulated pattern, were observed in livers of several MMA patients (Supplemental Figure 2B, a–c). The etiology and significance of this finding is currently unknown, but similar changes were not evident in the mouse livers.

Electron microscopy of the livers and kidneys confirmed the presence of various stages of mitochondrial pathology, including mitochondrial proliferation, formation of electron-lucent megamitochondria with shortened or absent cristae, and, in some cases, huge autophagic/lysosomal vacuoles containing degrading membrane material (Figure 2B and Supplemental Figure 2B, d–i). In the case of a severely affected older patient transplanted at age 24 years, large vacuoles with inclusions were prominent and spread throughout many sections of the liver (Supplemental Figure 2Bi), perhaps representing end-stage cellular structures.

Likewise, the murine renal pathology recapitulated the human patient observations. Light microscopy showed that *Mut*$^{-/-}$;*Tg*$^{INS\text{-}MCK\text{-}Mut}$ kidneys contained multifocal 2- to 4-micron eosinophilic vacuoles in the proximal tubules, consistent with proliferated, enlarged mitochondria (Supplemental Figure 4A, a–c). Plasma Lcn2 concentrations, a kidney disease biomarker previously described and validated in a large MMA patient cohort (27), were significantly elevated in the *Mut*$^{-/-}$;*Tg*$^{INS\text{-}MCK\text{-}Mut}$ mice compared with their heterozygote littermates and correlated with GFR measurements (Supplemental Figure 4, B and C).

Despite the significant growth failure and hepatorenal mitochondriopathy, *Mut*$^{-/-}$;Tg$^{INS\text{-}MCK\text{-}Mut}$ mice appeared and acted grossly normal; had normal serum biochemistries, except for increased alkaline phosphatase and decreased amylase (Supplemental Figure 5A); and showed no differences compared with heterozygote littermates when challenged with a glucose tolerance test (Supplemental Figure 5B).

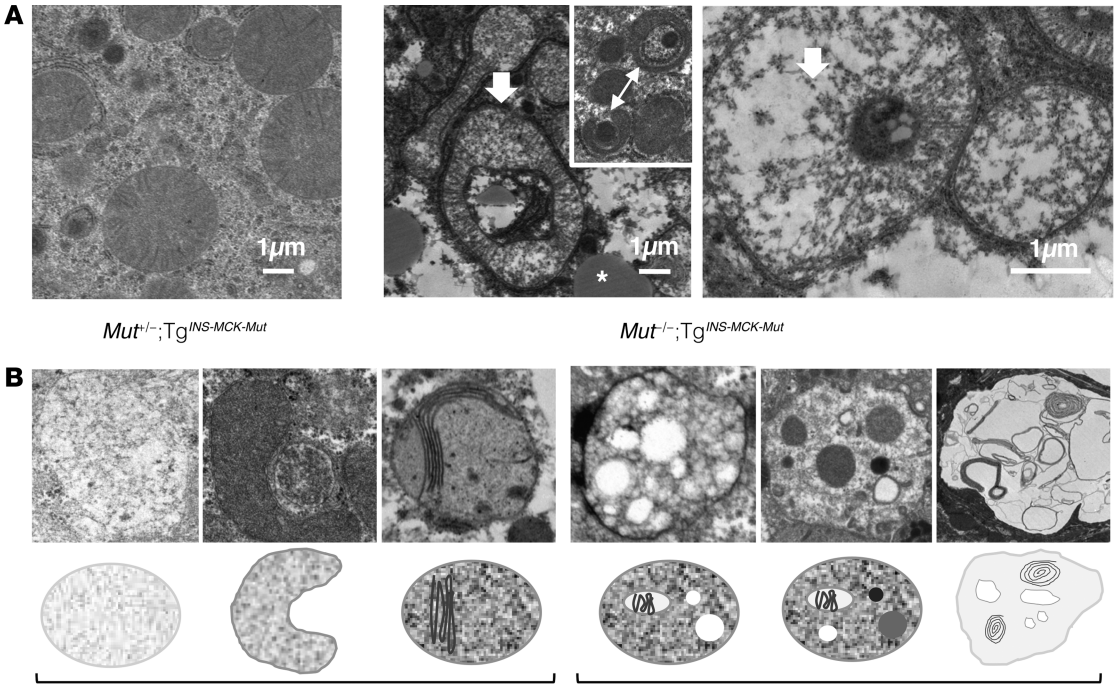

Figure 2. Hepatic ultrastructural changes in *Mut*$^{-/-}$;Tg$^{INS\text{-}MCK\text{-}Mut}$ animals replicate the pathology seen in MMA patients. (**A**) Electron microscopy of mutant mouse liver tissue showed lipid droplets (white asterisk, middle) and wide-spread large, abnormally shaped mitochondria with cristae rarefication and decreased matrix density in mutant animals (white arrows, middle and right), as opposed to their heterozygote littermates reared on the same diet (left) (scale bars: 1 μm). Many formed ring-shaped structures and appeared to be engulfing other cellular components (arrow with two heads, middle inset). (**B**) Ultrastructure of explanted livers from patients undergoing a liver transplantation procedure showed mitochondria with reduced matrix density and shortened, disorganized cristae and, in some cases, complex cytoplasmic inclusions of varying density engulfed by membranes, suggestive of autophagic vacuoles. Representative structural changes and a graphic of the observed pathology in the mitochondrial ultrastructure (left) and cellular autophagic vacuoles/inclusions (right) are depicted.

Finally, the overexpression of Mut in skeletal muscle did not alter tissue histology (Supplemental Figure 5C), and carriers of the INS-MCK-Mut transgene were normal in appearance, behavior, and fertility.

Hepatic adaptation to metabolic stress is abnormal in Mut$^{-/-}$;Tg$^{INS\text{-}MCK\text{-}Mut}$ mice. Given that metabolic decompensation in patients is typically preceded by reduced oral intake, we sought to mimic a crisis in the MMA mice using fasting stress. We compared hepatic gene expression profiles between male *Mut*$^{-/-}$;Tg$^{INS\text{-}MCK\text{-}Mut}$ mice at baseline and after fasting and included similar prepared samples from sex-matched *Mut*$^{+/-}$;Tg$^{INS\text{-}MCK\text{-}Mut}$ littermates (n = 4 per group). Male tissues were chosen for the microarray experiments because female *Mut*$^{-/-}$;Tg$^{INS\text{-}MCK\text{-}Mut}$ mice developed hypoglycemia, as compared with their male littermates, after 14 hours of fasting (Supplemental Figure 6A). Additional mouse tissues from a biological replicate study were used for subsequent qRT-PCR validation of the gene changes observed. Principal component analysis and fold change replicate analysis guided the selection of a 3-fold threshold for reliable discrimination. Although variability was larger in the comparison between *Mut*$^{-/-}$;Tg$^{INS\text{-}MCK\text{-}Mut}$ and *Mut*$^{+/-}$;Tg$^{INS\text{-}MCK\text{-}Mut}$ mice at baseline, expression differences were more homogenous in the fasting state, which was the main focus of our analysis (Supplemental Figure 6B).

Significant enrichment was identified in pathways involved in immune/inflammatory responses, including the LPS/IL-1–mediated inhibition of RXR function pathway (Table 1), which includes genes such as *Gstm3, Fmo3, Fabp5, CPT1B, Cyp2a12,* and *Abcc4*, which downregulate the hepatic metabolism of lipids, cholesterol, bile acids, and organic anion/xenobiotics through the secretion of IL-1 and TNF-α. Additional pathways that differed between mutant and heterozygote mice during fasting were those that mediate the acute phase response and complement system signaling (*Orm1*, *Saa4*, *Socs2*, *Saa2*, *C9*, *C6*), fatty acid metabolism (*Cyp2B13/9*, *Cpt1B*, *Cyp2A12/22*), steroid metabolism (*Hsd3b1*, *Cyp7b1*), and the cell cycle (*Myc*, *Ccnd1*) (Supplemental Tables 1 and 2). A subset of critical genes was validated by qPCR in the biological replicate study (Supplemental Figure 7 and Supplemental Table 3).

An expression profile consistent with a switch from fatty acid synthesis to gluconeogenesis was observed in the fasted mice and was accentuated in the mutant animals, which showed a marked upregulation in pyruvate dehydrogenase kinase, isoform 4 (*Pdk4*), both at baseline and after fasting compared with their heterozygote littermates. In contrast, *Gstm3,* a glutathione-*S*-transferase important in the detoxification of environmental toxins, drugs, carcinogens, and oxidative stress products, was a gene that, instead of being downregulated with fasting, was highly upregulated both at baseline and after fasting in the $Mut^{-/-}$;$Tg^{INS\text{-}MCK\text{-}Mut}$ mice. A similar expression pattern was observed for *Slc7a11* (xCT), a cystine/glutamate antiporter necessary for glutathione repletion during hepatic stress.

We subsequently focused on individual genes that showed a dissimilar response to fasting between heterozygote and mutant mice, hypothesizing that such genes may underlie the maladaptive response to stress seen in MMA patients and mice. One of the genes with a highly divergent response to fasting in $Mut^{-/-}$;$Tg^{INS\text{-}MCK\text{-}Mut}$ mice was *Fgf21*. *Fgf21* showed 41.23% ± 23.8% higher mRNA expression in the livers of the $Mut^{-/-}$;$Tg^{INS\text{-}MCK\text{-}Mut}$ mice compared with heterozygote and wild-type controls and was validated in a biological replicate as differentially expressed at the level of mRNA and in the plasma in $Mut^{-/-}$;$Tg^{INS\text{-}MCK\text{-}Mut}$ mice compared with littermate controls (Figure 3, A and B). However, instead of showing an induction with fasting, as seen in the heterozygote animals (3.3% ± 0.53% control from 1.25% ± 0.9%), *Fgf21* was substantially downregulated (17.5% ± 9.5% control, down from 41.23% ± 23.8%) (Figure 3A). Given the central role of the Fgf21 axis in mitochondrial metabolism, especially in mouse models characterized by resistance to diet-induced obesity (36, 37), this cytokine was chosen as a target for further studies in patients.

Plasma Fgf21 concentrations are modulated by hepatic Mut expression. To further explore Fgf21 as an MMA-associated disease biomarker, and possibly as an outcome parameter for future human treatment studies, we used mouse models to interrogate the influence of hepatic Mut expression on plasma Fgf21 levels via germ line transgenesis or gene addition. We first compared the $Mut^{-/-}$;$Tg^{INS\text{-}MCK\text{-}Mut}$ Fgf21 concentrations to those measured in the liver transgenic mice ($Mut^{-/-}$;$Tg^{INS\text{-}Alb\text{-}Mut}$) (27). Liver transgenic mice at 6 months of age had minimal elevations of plasma Fgf21 compared with the muscle transgenic animals at 3–4 months of age (Figure 3B). Concentrations were higher at weaning, even for some heterozygote animals, and then gradually increased after the first month in the muscle transgenic mice (Supplemental Figure 6C). Moreover, Fgf21 plasma concentrations remained largely unchanged (except for one sick outlier male mouse), even after a 2-month high-protein challenge in the liver transgenic mice, a dietary treatment that induces massive plasma metabolite elevations, with an accompanying significant decline in renal function in these mice (Figure 3B) (27).

Next, a canonical adeno-associated virus (AAV) gene therapy vector configured to express human MUT cDNA under the control of the ApoE-enhanced, human α 1 antitrypsin promoter/enhancer combination (AAV2/8 hAAT *MUT*) was packaged with a serotype 8 capsid (38) and systemically delivered via a retro-orbital injection at a dose of 5×10^{12} GC/kg (AAV genome copies/kg) to $Mut^{-/-}$;$Tg^{INS\text{-}MCK\text{-}Mut}$ mice at weaning. As expected, significant and durable improvements in the clinical and biochemical parameters were observed in the AAV8-treated mice. These animals showed substantial weight gain, an increase in whole body 1-^{13}C propionate oxidation, and a prolonged metabolic stability after gene therapy, as opposed to untreated control littermates (Figure 3, C and D, respectively). Notably, the biochemical and phenotypic correction of the $Mut^{-/-}$;$Tg^{INS\text{-}MCK\text{-}Mut}$ mice was associated with a massive decrease in plasma Fgf21 concentrations (Figure 3E) (90% decrease compared with baseline levels, from 4,084.6 ± 823.4 pg/ml to 643.1 ± 162.8 in 60 days and 1,130.6 ± 190.3 after 1 year), which paralleled the response of traditional biochemical markers, such as plasma methylmalonic acid (from 1,253 ± 216.8 μmol/l to 179.3 ± 4.8 in 60 days and 409 ± 27.7 after 1 year).

Elevated plasma FGF21 concentrations in MMA patients correlate with markers of disease severity and are ameliorated by LT. The mouse studies led us to analyze plasma FGF21 in clinical research samples collected from 72 patients with various subtypes of MMA (n = 58 with the *mut* subtype, 6 with *cblB*, and 8 with *cblA*; 1–5 samples per patient were tested for a total of 156 measurements) versus parental controls (n = 11) (Figure 4A). Samples were obtained during regular longitudinal protocol visits in the well state. Extreme elevations of plasma FGF21 were observed in mut^0 patients (6,430 ± 8,149 pg/ml, mean ± SD), as opposed to heterozygote parental control samples (73.6 ± 58.94 pg/ml, mean ± SD). Total and intact (active) FGF21 were measured in 38 samples (39). Intact FGF21 was 10%–120% of the respective total FGF21 values, (53.34% ± 27.4%, mean ± SD), while the Δ(total – intact) FGF21 showed a weak correlation (R^2 = 0.18, r = 0.42, P = 0.014), with the degree of renal dysfunction suggesting that part of the measured FGF21 in the extremely elevated samples was caused by decreased renal clearance of fractionated FGF21 (Supplemental Figure 8, A and B). Longitudinal measurements revealed a gradual increase in plasma FGF21 in mut^0 patients, who were referred for

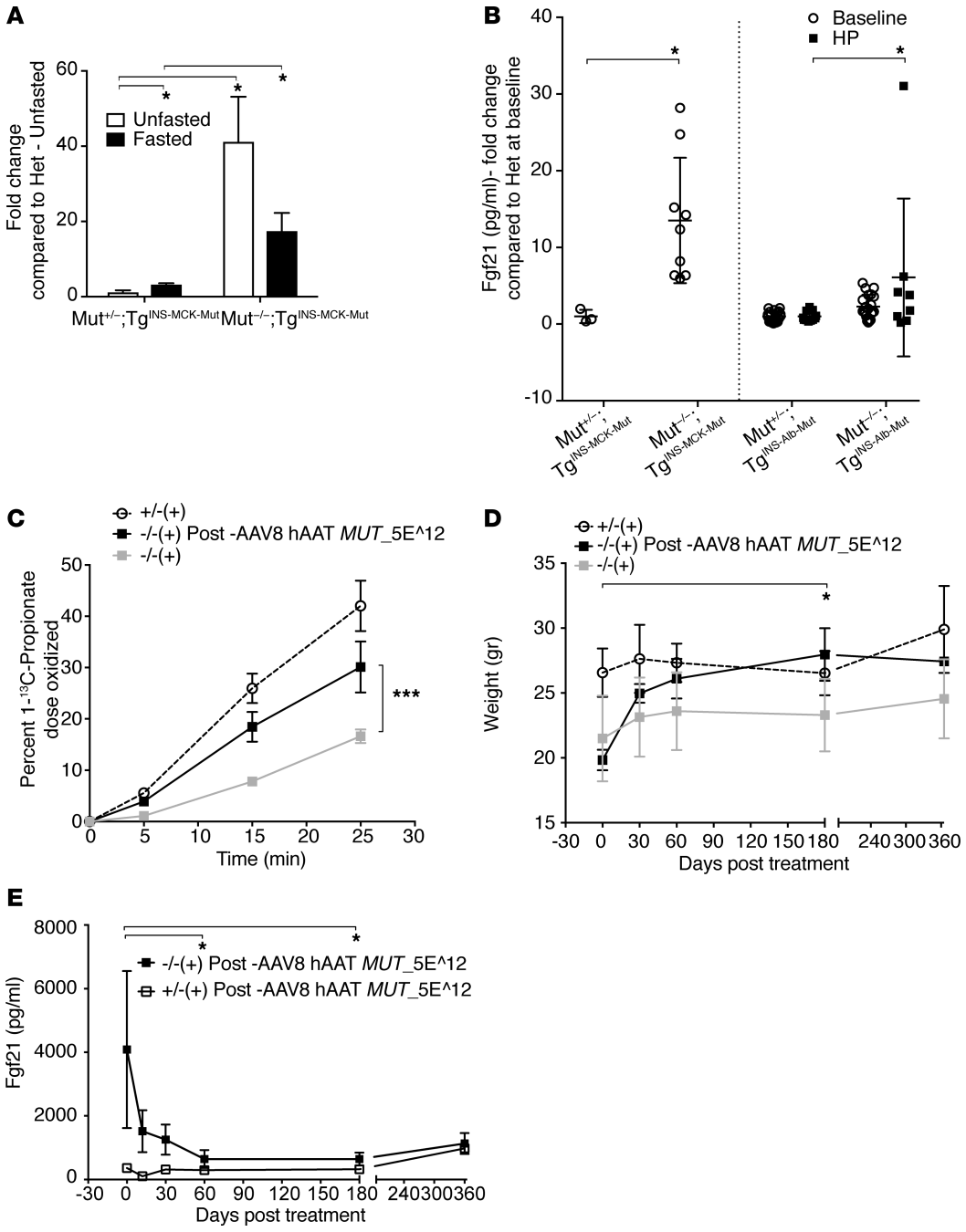

Figure 3. Fgf21 dysregulation in *Mut*$^{-/-}$;Tg$^{INS\text{-}MCK\text{-}Mut}$ mice. Hepatic *Mut* correction by transgenesis or AAV gene therapy confers biochemical and clinical improvement in *Mut*$^{-/-}$;Tg$^{INS\text{-}MCK\text{-}Mut}$ mice, associated with a precipitous decrease in Fgf21. (**A**) *Mut*$^{-/-}$;Tg$^{INS\text{-}MCK\text{-}Mut}$ mice had 41,237 ± 11.943 vs. 1.257 ± 0.47–fold higher hepatic *Fgf21* mRNA expression compared with heterozygous mice at baseline (white bars) but failed to induce its transcription in the fasting state (black bars) (n = 4 per group and condition tested). (**B**) Liver transgenic animals, *Mut*$^{-/-}$;Tg$^{INS\text{-}Alb\text{-}Mut}$ display milder elevations in plasma Fgf21 concentrations (2.282 ± 0.337–fold higher than their heterozygote littermates, n = 21 and 19, respectively, P = NS) that were relatively unaffected by high-protein challenge, except for a sick male mutant animal (6.07 ± 3.62–fold higher than controls, n = 8; P = NS). (**C**) A single retro-orbital injection of a 5 x 10^{12} GC/kg (AAV genome copies/kg) dose of the AAV8-hAAT-*MUT* vector conferred a robust increase in 1-^{13}C-sodium propionate oxidation in *Mut*$^{-/-}$;Tg$^{INS\text{-}MCK\text{-}Mut}$ mice compared with their baseline levels (30.122 ± 8.61 after gene therapy compared with 16.637 ± 4.012 at baseline, n = 3 and 9, respectively). (**D**) Liver-directed gene therapy caused a rapid weight gain in the treated mice (P = 0.015 at 180 days after gene therapy compared with pretreatment weights, n = 3, Friedman paired nonparametric ANOVA after correction for multiple comparisons). (**E**) Plasma Fgf21 concentrations ranged from 1,000–7,000 pg/ml (normal <200) before gene therapy. Serial repeat measures after gene therapy over a year showed a significant decrease in plasma Fgf21 compared with baseline at days 60 and 180 (adjusted P = 0.0228 and 0.0441, respectively, compared with day 0, Friedman nonparametric repeated-measures ANOVA with correction for multiple comparisons). *P < 0.05, ***P < 0.001.

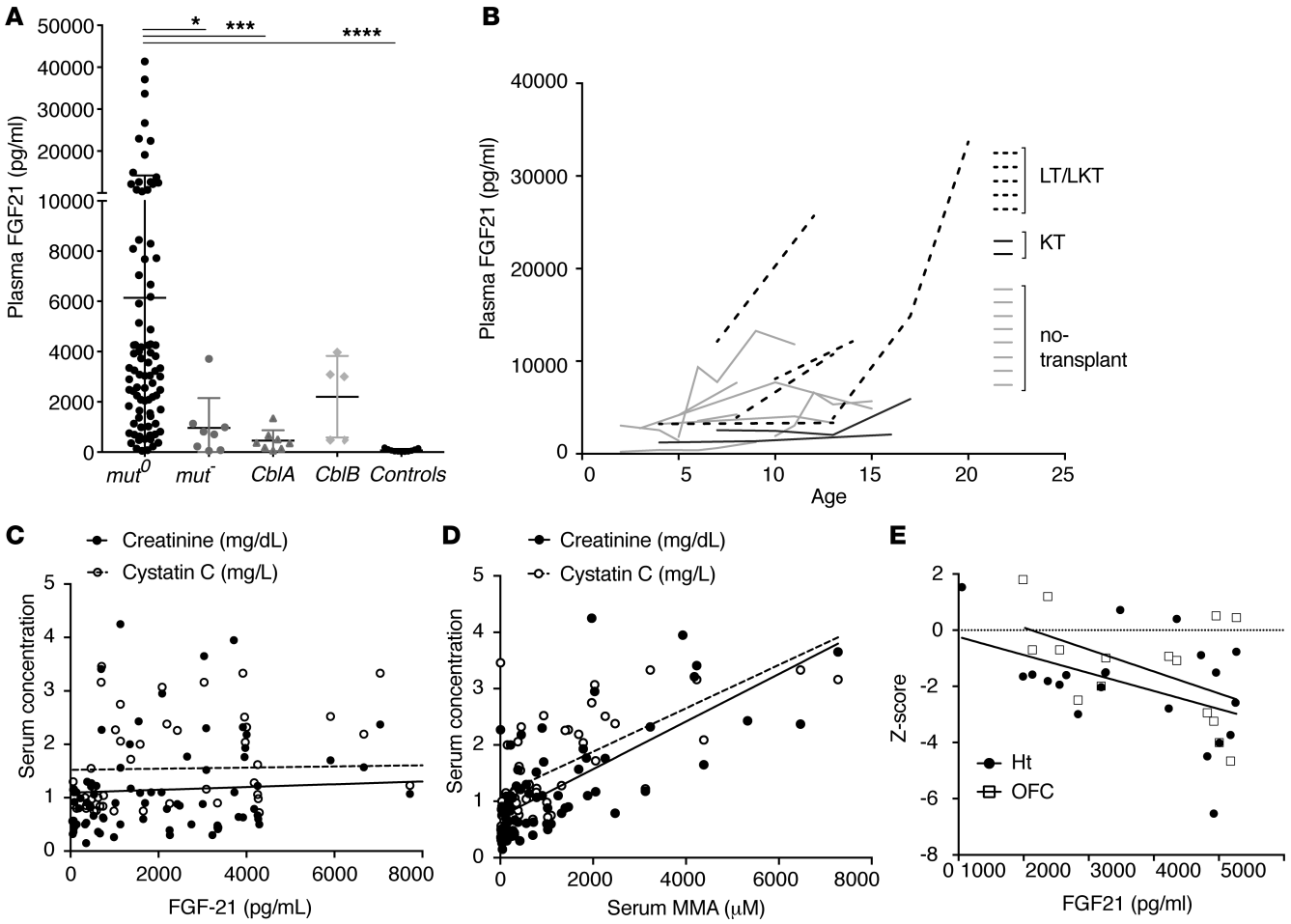

Figure 4. Plasma FGF21 concentrations in methylmalonic acidemia patients—correlations with subtype severity and clinical parameters. (**A**) FGF21 concentrations were massively elevated in MMA patients compared with controls (range: 355.9–41,371.06 pg/ml, mean ± SD; 6,430 ± 8,149 for *mut*^{0} patients, 965.4 ± 1,185 for *mut*$^-$ patients; 458.4 ± 412.2 in *cblA* patients; and 2,206 ± 1,662 in *cblB* patients, as opposed to 73.67 ± 58.94 in controls; n = 86, 8, 8, 5 and 11, respectively; $P < 0.0001$, Kruskal-Wallis test). Significant differences were observed between *mut*^{0} and all other subtypes, except the *cblB* (adjusted P values by Dunn's multiple comparisons test comparing each subtype to *mut*^{0} were 0.0145 for *mut*$^-$, 0.0009 for cblA, and <0.0001 for controls). Lowest concentrations were measured in *cblA* patients, who represent the milder, B12-responsive form of the disease. *$P < 0.05$, ***$P < 0.001$, ****$P < 0.0001$. (**B**) Longitudinal measurements reveal a gradual increase in plasma FGF21 in *mut*^{0} patients who were referred for liver and or liver/kidney transplantation (dotted lines), as opposed to isolated kidney transplant (dark gray lines) or no transplant (light gray lines). (**C**) FGF21 plasma concentrations showed no correlation with renal function indices, including serum creatinine (r = 0.1947, P = 0.079, R^2 = 0.0379, n = 82) and cystatin C (r = 0.0739, P = 0.587, R^2 = 0.0054, n = 56) (black and white circles, respectively). (**D**) In contrast, serum MMA (μM) shows a very strong correlation with renal function indices, serum creatinine (r = 0.708, $P < 0.0001$, R^2 = 0.50, n = 83) and cystatin C (r = 0.682, $P < 0.0001$, R^2 = 0.46, n = 57). (**E**) Plasma FGF21 concentrations showed a negative correlation with height-for-age Z-score (r = –0.455, P = 0.038, R^2 = 0.277) and head circumference-for-age Z-score (r = –0.505, P = 0.05, R^2 = 0.255).

LT and or LKT, as opposed to isolated kidney transplant or no transplant group (Figure 4B), with the highest level (> 40,000 pg/ml) measured in a patient who showed the most abnormal ultrastructural findings on electron microscopy examination (Supplemental Figure 2Bi). In 2 patients, FGF21 was measured before, during, and after a metabolic crisis. FGF21 showed a substantial upregulation during the episode of vomiting and metabolic ketoacidosis that required an inpatient admission for i.v. fluid replacement; concentrations returned to baseline upon discharge (Supplemental Figure 8C). FGF21 concentrations were similar between males and females and did not correlate significantly with age (data not shown). Importantly, in contrast to the direct effects of renal insufficiency upon serum methylmalonic acid levels (27, 40), FGF21 levels did not correlate significantly with creatinine or cystatin C in the patients studied (Figure 4C, compared with the correlation with serum MMA concentrations, Figure 4D).

The relation of FGF21 concentrations to disease severity was further explored in patients with *mut*^{0} MMA, where correlations to other clinical outcomes and laboratory indices, such as growth (height Z-score: r = –0.455, P = 0.038, R^2 = 0.277; head circumference Z-score: r = –0.505, P = 0.05, R^2 = 0.255;

Figure 4E), plasma amino acids (glycine and alanine; Supplemental Figure 8D), and oxidative stress biomarkers (urine F2iP; Supplemental Figure 8E) were observed. Given the role of FGF21 during fasting, it was not surprising to observe a negative association with plasma concentrations of the essential BCAA, valine (plasma valine: $r = –0.345$, $P = 0.031$, $R^2 = 0.119$; Supplemental Figure 8F).

Finally, a cohort of MMA patients who received LT or combined LKT were studied and compared to a smaller group who received kidney-only transplants. LT or combined LKT patients experienced a significant drop in serum methylmalonic acid concentrations but an even more dramatic fold change in the plasma FGF21 concentrations (Figure 5A). A uniform and sustained decrease was observed in LT/LKT recipients spanning a period of up to nearly 20 years after transplant (Figure 5B), with a late increase more than 15 years after LKT observed in a *mut*^{0} patient who only received a *partial* auxiliary liver transplant and in a second patient with morbid obesity and likely fatty liver changes in the transplanted liver. Similarly, 2 severe *mut*^{0} patients, of the 5 who received an isolated kidney transplant, showed a continuing increase in plasma FGF21 concentrations, suggesting a ongoing progression of liver disease in the patient native *mut*^{0} MMA liver (Figure 5C). Both patients experienced a number of metabolic decompensations despite receiving a renal allograft and eventually progressed to renal failure after 2 and 6 years, respectively. Finally, the differences between LT/LKT versus KT recipients further support that the remarkable decrease of plasma FGF21 in liver transplant recipients was not merely an effect of the immunosuppressive/antirejection medications they received after transplant, since KT recipients were on a similar medication regimen. Collectively, these data show that FGF21 levels will be a clinically useful biomarker of disease severity in MMA and could be used to track a response to hepatic-directed therapies.

Discussion

In the current work, we relied upon the expression of Mut in the skeletal muscle to generate a viable model of the hepatorenal syndrome that characterizes MMA in humans (23, 41), to both create a permissive environment for the study of disease pathophysiology and allow the testing of liver-targeted therapies (27, 42, 43). Indeed, *Mut*$^{-/-}$;Tg$^{\text{INS-MCK-}Mut}$ mice have been used in proof-of-concept preclinical testing of systemic mRNA enzyme replacement therapy for MMA (44). Although transgenic overexpression of *Mut* protected *Mut*$^{-/-}$ mice from neonatal lethality and was accompanied by an increased activity of Mut in the skeletal muscle, it conveyed only a small increase in whole body 1-^{13}C-propionate oxidation. In contrast, a much smaller level, approximately 8%, of hepatic *Mut* mRNA expression, provided as a transgene using the same *Mut* cDNA under the control of the albumin promoter, conferred near normal 1-^{13}C propionate oxidation in the liver transgenic MMA mouse model (Supplemental Figure 1D). The disparate metabolic phenotypes observed after tissue-specific correction likely reflect the intrinsic ability of muscle and liver mitochondria to fix propionate into propionyl-CoA. Skeletal muscle mitochondria, in contrast to those from hepatocytes, have a limited capacity to fix propionate to propionyl-CoA (45), which likely underlies the different toxicities observed in the respective cells and phenotypic effects observed after tissue-specific transgenesis. For example, in a related model of *Mut* deficiency, hepatic megamitochondria formation and electron transport chain dysfunction were characteristic, but skeletal muscle mitochondria were unremarkable, both ultrastructurally and enzymatically (23). While our studies support the concept that skeletal muscle has a limited capacity to metabolize propionate, the fact the muscle-directed *Mut* expression results in uniform rescue from the neonatal lethality displayed by *Mut*$^{-/-}$ mice is consistent with the role that muscle plays in the oxidation of BCAAs, including valine and isoleucine, which are claimed to contribute to approximately 40% of the metabolic load in patients with MMA (46).

Despite their improved survival, the *Mut*$^{-/-}$;Tg$^{\text{INS-MCK-}Mut}$ mice were fragile, required a HFCD to survive, and remained significantly smaller than their littermates throughout their life span. Very similar to what we and others have documented in MMA patients (27–29, 47), these mice uniformly manifest severe hepatorenal mitochondrial pathology, which was accompanied by a cytochrome *c* oxidase deficiency and renal insufficiency. The combined observations in mice and patients with MMA reveal that the mitochondrial changes in the hepatocytes and proximal tubules are progressive and, at end stage, feature giant inclusions reminiscent of structures seen when mito/autophagy is deranged (48–50). While *Mut*$^{-/-}$;Tg$^{\text{INS-MCK-}Mut}$ mice displayed grossly normal activity levels and overall behavior, they were extremely sensitive to stressors, such as retro-orbital bleeding, fighting, or cage flooding. During life, the animals also exhibited severe failure to thrive, yet had normal appetite and ingestion. Thus, the mice recapitulate the key recognized microscopic and phenotypic features of the human condition, such as mitochondrial dysfunction and growth failure,

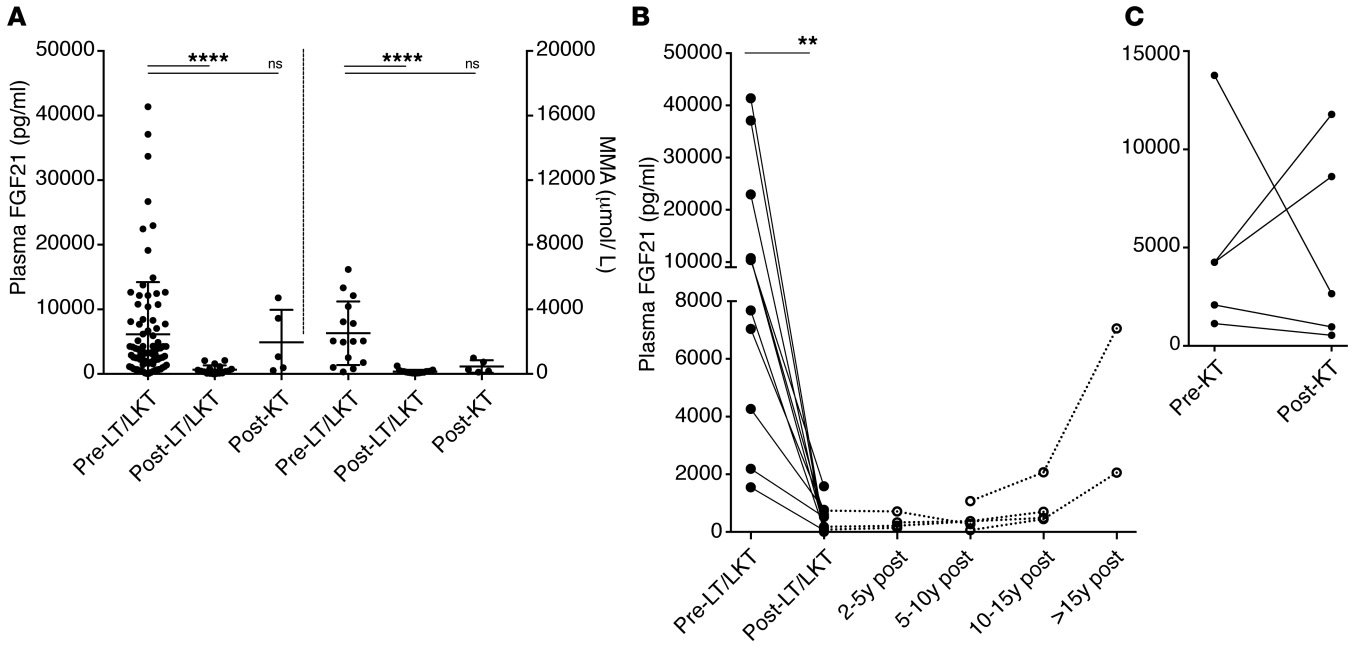

Figure 5. Plasma FGF21 response to organ transplantation. (**A**) Liver or combined liver and kidney but not isolated kidney transplant recipients had a significant lower plasma FGF21 concentrations than nontransplanted *mut*^{0} patients (mean ± SEM; 13,953 ± 12,611 pg/ml vs. 467.8 ± 522.9, $n = 10$; $P < 0.002$, paired Wilcoxon test). The fold change in FGF21 was more significant than the change in plasma methylmalonic acid concentrations (from 2,854 ± 2,452 to 298.4 ± 171.9; $P < 0.0059$; $n = 10$). (**B**) FGF21 plasma concentrations measured before and after LT/LKT ($n = 12$) showed uniform and sustained improvement. A late increase more than 15 years after LKT was observed in a *mut*^{0} patient, who received a partial auxiliary liver transplant and a second case with morbid obesity. (**C**) Kidney transplant recipients ($n = 5$) experienced a varied response in plasma FGF21 levels. Two patients showed increased FGF21, correlating with the severity of their disease progression.

despite provision of a high-calorie food composed primarily of fat and carbohydrates, similar to the diet consumed by patients (13, 35).

Another hallmark of MMA, and related organic acidemias, is the propensity for patients to suffer from metabolic crises, which are typically precipitated after diminished oral intake during an intercurrent illness. We therefore sought to explore the mechanisms underlying metabolic instability by exposing the *Mut*$^{-/-}$;Tg$^{\text{INS-MCK-}Mut}$ mice to a fasting challenge and then pursued genomic studies to characterize the hepatic response. Gene expression analysis in the fasted state showed differential clustering in a number of pathways, with significant enrichment of genes involved in drug metabolism and immune/inflammatory responses. Upregulated transcripts included phase I or II enzymes that function in the metabolism and elimination of organic acids, the cytochrome P450 (CYP) enzyme system, and related genes, as well as glutathione-*S*-transferase (*Gstm3)*, an enzyme involved in detoxification of environmental toxins, and *Slc7a11*, encoding the cystine/glutamate antiporter (xCT) that imports cystine, a precursor needed for glutathione synthesis, an important pathway for liver regeneration (51). In aggregate, these gene products are likely needed to process the massive flux of endogenous toxins accumulating as a result of the block, such as propionate, methylmalonate, and the corresponding coenzyme A esters, to protect against oxidant injury and/or promote liver repair. A marked induction of genes that are involved in rate-controlling steps in both lipid and glucose metabolism, *Cpt1B* and *Pdk4*, was documented. These pathways are tightly regulated by PPARα, the key orchestrator of the switch from the fed to the fasted condition via activation of fatty acid catabolism and neoglycogenesis. Thus, the pattern of adaptation in the MMA hepatocyte is characterized by increased expression of genes involved in the disposal of "toxic" metabolites, cell survival, liver regeneration, and an oxidant stress response, with an accompanying transcriptional signature of metabolic rechanneling of lipid and glucose metabolism. Because similar pathways are implicated in the etiology of nonalcoholic fatty liver disease and steatohepatitis (52–54), conditions which MMA patients may be prone to develop (47), these differentially regulated genes, as a group, may harbor fruitful targets for small-molecule modulation.

Despite the dependence on HFCD diets throughout their life span, and in the patients coexisting obesity (13), neither MMA mice nor patients are recognized to display the metabolic syndrome phenotype or develop early type 2 diabetes. In fact, glucose tolerance was normal in the MMA mice but not directly

Table 1. Pathway enrichment analysis of gene groups differentially expressed in the fasting state

Canonical pathway name	–log (*P* value)
Immune responses	
LPS/IL-1–mediated inhibition of RXR function	4.17E-05
Acute phase response signaling	2.00E-04
Complement system	5.01E-03
Metabolic processes	
Tryptophan metabolism	7.94E-04
Nitrogen metabolism	6.03E-03
Metabolism of xenobiotics by cytochrome P450	6.03E-03
Fatty acid metabolism	7.08E-03
Aryl hydrocarbon receptor signaling	9.77E-03
Linoleic acid metabolism	2.45E-02
Androgen and estrogen metabolism	2.63E-02
Cell regulation and proliferation	
Thyroid cancer signaling	3.80E-04
Endometrial cancer signaling	1.23E-02
Cell cycle – G_1/S checkpoint regulation	1.41E-02
Small cell lung cancer signaling	2.19E-02
Prolactin signaling	2.34E-02
Acute myeloid leukemia signaling	2.57E-02
Bladder cancer signaling	3.39E-02
Chronic myeloid leukemia signaling	3.72E-02

RXR, retinoid X receptor.

assessed in patients, because in nontransplanted cases studied longitudinally under a natural history protocol, HbA1c was normal and did not correlate with BMI (data not shown). It was therefore intriguing to discover *Fgf21*, a key metabolic regulator with antihyperglycemic, antihyperlipidemic, and thermogenic properties (37), as the most significantly dysregulated gene in the MMA mice. Human FGF21 is a 181–amino acid peptide (~22.3 kDa), derived from a 208–amino acid mature precursor. FGF21 has pleiotropic metabolic effects, mediated in part through a unique coreceptor, β-klotho, which is expressed in selected tissues, including the liver, white adipose tissue, and pancreas. As a downstream target of PPARα and SIRT1, FGF21 mediates protection against hepatic steatosis and enhances expression of brown fat–like genes in white adipose tissue, increasing whole-body energy expenditure (55–59). While *Fgf21*$^{-/-}$ mice display impaired hepatic fatty acid oxidation gene expression and blunted ketogenesis, transgenic mice overexpressing Fgf21 in the liver are resistant to diet-induced obesity (60), an observation that aligns with the beneficial antimetabolic syndrome effects seen in mice or primates after receive FGF21 by systemic administration (61, 62). Because Fgf21 levels were massively (10- to 100-fold) increased in both MMA mice and patients, but not in littermates fed the same diet or parental controls, it seems likely that the Fgf21 response we have documented in MMA could contribute to protection against the untoward effects of dysregulated metabolism and explain why the patients, who are often obese, overfed, and underactive (35), are not recognized to develop early type 2 diabetes.

Plasma FGF21 concentrations measured in our MMA patient cohort are 4- to 10-fold higher than those previously reported in studies of children and adults with a range of inborn errors of metabolism, including organic acidemias (63), mitochondrial myopathies, nonalcoholic fatty liver disease, or other disease states (64–67), and corresponded to the disease subtype severity, with the lowest concentrations observed in patients with the B12-responsive *cblA* subtype and the highest levels seen preoperatively in 2 liver transplant recipients, 1 of whom had the most severe hepatic mitochondrial ultrastructural perturbations (Supplemental Figure 2Bi) noted in our cohort. Several other clinical and biochemical parameters were shown to correlate with plasma FGF21, including somatic growth indices (height- and occipitofrontal circumference-for-age *Z*-scores), oxidative stress markers (plasma alanine and glycine and urine F2-isoprostanes), and amino acids (data shown for valine in Supplemental Figure 8D). Of great importance to the consideration of FGF21 as a hepatic biomarker for MMA patients, where renal disease directly influences

the serum levels of methylmalonic acid, FGF21 concentrations did not correlate with renal disease indices, including creatinine, cystatin C, and estimated GFR, suggesting that circulating FGF21 will be a particularly useful biomarker to track hepatic mitochondrial dysfunction and response to MUT replacement therapies, independent of kidney function. A study published while the current work was under review further validates the correlations between plasma FGF21 and disease severity and lack of strong association with renal dysfunction in MMA patients (68). Because FGF21 is a pancreatic secretagogue (69) and increases bone loss (70, 71), additional roles in the pathophysiology of MMA mediated by FGF21, such as the propensity toward pancreatitis and low bone density, seem likely.

The chronic induction of FGF21 in response to the cellular stress of MMA, perhaps originally induced as an adaptive response to promote survival, was accompanied by basal activation of many other pathways central to intermediary metabolism. The general concept that an adaptive response to mild stress can be protective is termed hormesis, and when specifically concerning the mitochondria, mitohormesis (72–74), a term that quite appropriately describes the episodic nature of the "intoxication" group of inborn errors of metabolism, such as the prototypical organic acidurias MMA and propionic acidemia, where the patients suffer from frequent episodes of acute on chronic metabolic imbalance. While chronic mitochondrial stress activates a nuclear program of adaptation that could be protective, superimposed acute demands, such as an infection, surgery, or increased catabolism, are not tolerated due to an inability to further activate a compensatory response (75). The response to a fasting challenge in *Mut*$^{-/-}$;Tg$^{\text{INS-MCK-}Mut}$ mice supports this hypothesis because many of the genes normally induced by fasting were already greatly overexpressed compared with their heterozygote littermates at baseline and failed to show an additional increase or, as with FGF21, showed a reverse response in the fasting state. Chronically elevated Fgf21 in MMA mice may exert beneficial metabolic effects that protect them from diet-induced obesity, glucose intolerance, and other sequelae of the metabolic syndrome (76, 77), while the acute-on-chronic stressors exhaust mitocellular reserves, resulting in acute decompensation, which is eventually harmful to the cell/organ system. Similar hormetic effects have been suggested for reactive oxidative species and hypoxia in the treatment of mitochondrial disorders (78–80). Further collection of FGF21 levels in parallel with the longitudinal assessment of MMA patients will help characterize the relation of this marker to outcomes and associated comorbidities in this population (64, 67). Dissection of the pathways and markers that mediate the mitohormetic adaptation that we have begun to document in MMA should also help inform the timing and dosing of novel therapeutic interventions designed to prevent acute and long-term disease-related complications.

Using transgenic mice, patient biospecimens from a large natural history cohort, and proof-of-concept liver-directed AAV gene therapy, we were also able to demonstrate that plasma FGF21 can serve, along with 1-^{13}C-propionate oxidation and serum methylmalonic acid concentration, as a surrogate biomarker to track efficacy of liver-targeted therapies for MMA. After AAV8 MUT gene therapy, treated *Mut*$^{-/-}$;Tg$^{\text{INS-MCK-}Mut}$ mice demonstrated a rapid improvement in weight gain, improved 1-^{13}C-propionate oxidation, and a drastic reduction in plasma Fgf21, which paralleled the decline of the disease-specific metabolite, methylmalonic acid. The murine studies suggest that, in MMA patients, plasma FGF21 and 1-^{13}C-propionate oxidative capacity will emerge as useful outcome biomarkers, especially since serum methylmalonic acid concentrations can be influenced by impaired renal function (40). In patients, the plasma FGF21 levels normalized in recipients of LT/LKT but not after an isolated KT, despite being treated with similar antirejection medication regimens. The aggregate observations suggest that FGF21 concentrations may be used to help identify severely affected patients and serve as a surrogate biomarker to follow the hepatic response to therapy, as we show here is feasible in mice and patients.

Methods

Patients. Clinical data derived from the natural history protocol were available for correlations, including dietary information (Kcal/d, complete/deficient protein g/kg/d), and individual amino acid intake (13), resting energy expenditure measured by open-circuit indirect calorimetry (Deltatrac equipment; VIASYS), plasma quantitative amino acids, acylcarnitine profiles, plasma and urine methylmalonic acid, renal function biomarkers, and other biochemical data.

Mouse studies. Animals were housed in an AAALAC-accredited SPF facility and maintained on a 12:12-hour light-dark cycle (see Supplemental Methods for additional details).

Generation of Mut$^{-/-}$*;Tg*$^{\text{INS-MCK-}Mut}$ *mice*. *Mut*-knockout mice harboring a deletion of exon 3 in the *Mut* gene have been described previously (30, 81). Mice homozygous for this mutation (C57BL/6 *Mut* $^{-/-}$) lack *Mut*

mRNA, protein, and enzymatic activity and display immediate neonatal lethality unless rescued with various gene therapy vectors. A skeletal muscle–specific transgene, $Tg^{INS\text{-}MCK\text{-}Mut}$, was engineered to express the murine *Mut* gene under the control of the murine MCK promoter in skeletal and cardiac muscle, as previously described (32, 82). The p3300MCK-CAT plasmid was a generous gift of Stephen D. Haushcka, University of Washington, Seattle, Washington, USA. The construct was subcloned into the pINSbsMCM reverse clone, which is flanked by chicken β-globin 5′ HS4 insulator elements to suppress position effect variegation. The 5′ intron of the MCK promoter was not included. Founder C57BL/6 animals were screened for the presence of the INS-MCK-Mut transgene and bred to C57BL/6 mice to test transmission. Transgenic carrier mice were then bred with heterozygous mice of the *Mut*-knockout line to generate $Mut^{-/-}$;$Tg^{INS\text{-}MCK\text{-}Mut}$ mice. The mice were made from SV129OLA ES cells, and backcrossed for >10 generations onto C57BL/6.

Fasting study. Ten male (4 mutant and 6 heterozygote mice) and nine female (3 mutant and 6 heterozygote littermates) mice underwent a fasting challenge. Mice were deprived from food but had free access to water throughout the fasting study. Food was removed at 12:00 pm and blood glucose, body temperature, and weight were monitored every 3 hours for 9 hours, followed by every 2 hours, unless a drop in blood glucose or change in temperature or overall activity levels and behavior of the animal was observed, at which point more frequent monitoring was initiated. The experiment was terminated and mice were euthanized once glucose levels dropped to ≤45 mg/dl. That occurred after 16 hours in 3 female mice that had lower body weights at baseline (14.6 ± 6.6 g, mean ± SD). The average body weight for the male mice was 19.57 ± 2.3 g, and they all tolerated the fasting well. Males were sacrificed at the same time as the females for blood and tissue collection for gene expression studies. Tissues were snap-frozen in liquid nitrogen for RNA extraction, and terminal blood sampling was obtained for metabolomic and targeted biochemical studies.

AAV production and delivery. An AAV vector was prepared using an ApoE-enhanced, human α-1 antitrypsin (hAAT) promoter to drive the expression of a codon-optimized human MUT cDNA (synMUT) as described previously (38). The resulting hAAT MUT AAV was packaged into an AAV8 capsid (76), purified on an iodixanol gradient, and titered by qPCR as previously described (83) (see Supplemental Methods). Viral particles were suspended phosphate-buffered saline and delivered via retro-orbital injection at a dose of 5×10^{12} GC/kg.

Trial registration. This clinical study is registered in www.clinicaltrials.gov (NCT00078078; http://clinicaltrials.gov/ct2/show/NCT00078078).

Data deposition. The data reported in this paper have been deposited in the Gene Expression Omnibus (GEO) database (GSE118862).

Statistics. All data were recorded and prepared for analysis with standard spreadsheet software (Microsoft Excel). Statistical analysis was completed using Microsoft Excel, Prism 5 (GraphPad), or IBM SPSS version 21 statistical software. Data are presented as the mean ± SEM, with at least 3 animals or subjects. When applicable, a 2-tailed Student's *t* test or 1-way ANOVA was performed, followed by Bonferroni or Tukey-Kramer post hoc test for multiple comparisons. Kruskal-Wallis 1-way ANOVA testing was used when groups were of different sizes. Pearson's correlation coefficient and linear regression were used to establish correlations, and Kaplan-Meier analyses were performed on survival. A *P* value of less than 0.05 was considered significant.

Study approval. Patient studies were approved by the National Human Genome Research Institute Institutional Review Board as part of the NIH study "Clinical and Basic Investigations of Methylmalonic Acidemia and Related Disorders" (Clinicaltrials.gov, NCT00078078) and performed in compliance with the Declaration of Helsinki. Patients or their parents/legal guardians provided informed consent. All experiments were performed in agreement with NIH guidelines and with the approval of the Animal Care and Use Committees of the National Human Genome Research Institute and National Institute of Diabetes and Digestive and Kidney Diseases.

Author contributions

IM designed and performed mouse model experiments for characterization, GFR measurement, mouse and human histology, fasting challenge, microarray experiments, gene expression validation, FGF21 mouse and human measurements, clinical data preparation, statistical analysis, and figure and manuscript preparation. JRS performed mouse model characterization, fasting experiments, microarray studies, GFR, and propionate oxidation studies. MWE and CW assisted with the mouse model characterization and ELISAs on mouse and patient samples. MWE helped with manuscript preparation. Lina Li and RJC performed gene therapy experiments. YPK performed stable isotope mouse studies.

JLS, AP, and JG helped with the natural history protocol and clinical sample collection and performed ELISA assays, data collection, and statistical analysis. Lingli Li and JS helped with mouse GFR data analysis and interpretation. NST and AGE performed hepatic microarray experiments, analysis, and interpretation. BO performed and CLG supervised mouse MCM tissue activity measurements. PMZ, VH, MAA, MGT, and DEK performed histology and electron microscopy in mouse and human tissues and helped with interpretation. CG and SD performed mitochondrial immunohistochemistry. KCO and GME shared human liver tissues from transplant recipients. HJV, HCA, and SG referred critical patients and shared patient serum samples for biomarker validation. EAM and LHV prepared the AAV8 virus for the gene therapy experiments. CPV constructed mouse models and then conceived and supervised the entire study. IM and CPV wrote the manuscript, which was reviewed by all authors.

Acknowledgments

The authors dedicate this manuscript to the memory of Lara Williams-Lourenco for her significant contributions to MMA research.

The authors thank all patients and their families for their participation in our natural history protocol and donation of samples and tissues for our studies; referring physicians, nurses, and dietitians for their help with patient evaluations; Shelley Hoogstraten-Miller for outstanding veterinary support; Irene Ginty, Cherry Yang, Tina Aroyo, Theresa Ferrine, Lemlem Alemu, and Darwin Romero for their skilled assistance with mouse maintenance; Isa Bernardini and Roxanne Fischer for processing patient samples; the nurses and research dietitians of the NIH Clinical Research Center and clinical fellows of the National Human Genome Research Institute genetics fellowship program for their help with patient care and dedication to clinical research. We thank Julia Fekecs for her assistance with manuscript figure preparation. The authors want to acknowledge the "Angels for Alyssa," "A Cure for Clark," and the Organic Acidemia Association, nonprofit organizations founded by families and friends of patients with MMA, for their ongoing dedication and support of MMA research. This study was supported by the Intramural Research Program of the National Human Genome Research Institute, NIH. HJV was supported by NIH grant 1K08HD073492.

Address correspondence to: Charles P. Venditti, National Human Genome Research Institute, National Institutes of Health, Building 10, Room 7N248A, Bethesda, Maryland 20892-4442, USA. Phone: 301.496.6213; Email: venditti@mail.nih.gov.

1. Flavin M, Ortiz PJ, Ochoa S. Metabolism of propionic acid in animal tissues. *Nature*. 1955;176(4487):823–826.
2. Lardy HA, Adler J. Synthesis of succinate from propionate and bicarbonate by soluble enzymes from liver mitochondria. *J Biol Chem*. 1956;219(2):933–942.
3. Fenton WA, Hack AM, Willard HF, Gertler A, Rosenberg LE. Purification and properties of methylmalonyl coenzyme A mutase from human liver. *Arch Biochem Biophys*. 1982;214(2):815–823.
4. Mancia F, Evans PR. Conformational changes on substrate binding to methylmalonyl CoA mutase and new insights into the free radical mechanism. *Structure*. 1998;6(6):711–720.
5. Banerjee R. Radical carbon skeleton rearrangements: catalysis by coenzyme B12-dependent mutases. *Chem Rev*. 2003;103(6):2083–2094.
6. Wilkemeyer MF, Andrews ER, Ledley FD. Genomic structure of murine methylmalonyl-CoA mutase: evidence for genetic and epigenetic mechanisms determining enzyme activity. *Biochem J*. 1993;296 (Pt 3):663–670.
7. Stokke O, Eldjarn L, Norum K, Steen-Johnsen J, Halvorsen S. Methylmalonic acidemia: a new inborn error of metabolism which may cause fatal acidosis in the neonatal period. *Scand J Clin Lab Invest*. 1967;(20):313–328.
8. Oberholzer VG, Levin B, Burgess EA, Young WF. Methylmalonic aciduria. An inborn error of metabolism leading to chronic metabolic acidosis. *Arch Dis Child*. 1967;42(225):492–504.
9. Rosenberg LE, Lilljeqvist AC, Hsia YE. Methylmalonic aciduria. An inborn error leading to metabolic acidosis, long-chain ketonuria and intermittent hyperglycinemia. *N Engl J Med*. 1968;278(24):1319–1322.
10. Matsui SM, Mahoney MJ, Rosenberg LE. The natural history of the inherited methylmalonic acidemias. *N Engl J Med*. 1983;308(15):857–861.
11. Manoli I, Sloan JL, Venditti CP. Isolated Methylmalonic Acidemia. In: Pagon RA, et al. eds. GeneReviews(R). Seattle,WA; University of Washington:1993.
12. Baumgartner MR, et al. Proposed guidelines for the diagnosis and management of methylmalonic and propionic acidemia. *Orphanet J Rare Dis*. 2014;9:130.
13. Manoli I, Myles JG, Sloan JL, Shchelochkov OA, Venditti CP. A critical reappraisal of dietary practices in methylmalonic acidemia raises concerns about the safety of medical foods. Part 1: isolated methylmalonic acidemias. *Genet Med*. 2016;18(4):386–395.
14. Fraser JL, Venditti CP. Methylmalonic and propionic acidemias: clinical management update. *Curr Opin Pediatr*. 2016;28(6):682–693.

15. Aldubayan SH, Rodan LH, Berry GT, Levy HL. Acute illness protocol for organic acidemias: methylmalonic acidemia and propionic acidemia. *Pediatr Emerg Care*. 2017;33(2):142–146.
16. Hörster F, et al. Long-term outcome in methylmalonic acidurias is influenced by the underlying defect (mut0, mut-, cblA, cblB). *Pediatr Res*. 2007;62(2):225–230.
17. Niemi AK, et al. Treatment of methylmalonic acidemia by liver or combined liver-kidney transplantation. *J Pediatr*. 2015;166(6):1455–61.e1.
18. Sloan JL, Manoli I, Venditti CP. Liver or combined liver-kidney transplantation for patients with isolated methylmalonic acidemia: who and when? *J Pediatr*. 2015;166(6):1346–1350.
19. van 't Hoff WG, et al. Combined liver-kidney transplantation in methylmalonic acidemia. *J Pediatr*. 1998;132(6):1043–1044.
20. Kasahara M, et al. Current role of liver transplantation for methylmalonic acidemia: a review of the literature. *Pediatr Transplant*. 2006;10(8):943–947.
21. Chen PW, et al. Stabilization of blood methylmalonic acid level in methylmalonic acidemia after liver transplantation. *Pediatr Transplant*. 2010;14(3):337–341.
22. Brosnan JT, Brosnan ME. Branched-chain amino acids: enzyme and substrate regulation. *J Nutr*. 2006;136(1 Suppl):207S–211S.
23. Chandler RJ, et al. Metabolic phenotype of methylmalonic acidemia in mice and humans: the role of skeletal muscle. *BMC Med Genet*. 2007;8:64.
24. Manoli I, Venditti CP. Branched Chain Amino Acid Metabolism. In: Lee B, Scaglia F, eds. *Inborn Errors of Metabolism: From Neonatal Screening to Metabolic Pathways*. New York, NY: Oxford University Press; 2015:92–118.
25. Okun JG, et al. Neurodegeneration in methylmalonic aciduria involves inhibition of complex II and the tricarboxylic acid cycle, and synergistically acting excitotoxicity. *J Biol Chem*. 2002;277(17):14674–14680.
26. Chandler RJ, et al. Mitochondrial dysfunction in mut methylmalonic acidemia. *FASEB J*. 2009;23(4):1252–1261.
27. Manoli I, et al. Targeting proximal tubule mitochondrial dysfunction attenuates the renal disease of methylmalonic acidemia. *Proc Natl Acad Sci USA*. 2013;110(33):13552–13557.
28. Zsengellér ZK, et al. Methylmalonic acidemia: a megamitochondrial disorder affecting the kidney. *Pediatr Nephrol*. 2014;29(11):2139–2146.
29. Wilnai Y, Enns GM, Niemi AK, Higgins J, Vogel H. Abnormal hepatocellular mitochondria in methylmalonic acidemia. *Ultrastruct Pathol*. 2014;38(5):309–314.
30. Chandler RJ, Venditti CP. Adenovirus-mediated gene delivery rescues a neonatal lethal murine model of mut(0) methylmalonic acidemia. *Hum Gene Ther*. 2008;19(1):53–60.
31. Wilkemeyer MF, Crane AM, Ledley FD. Primary structure and activity of mouse methylmalonyl-CoA mutase. *Biochem J*. 1990;271(2):449–455.
32. Johnson JE, Wold BJ, Hauschka SD. Muscle creatine kinase sequence elements regulating skeletal and cardiac muscle expression in transgenic mice. *Mol Cell Biol*. 1989;9(8):3393–3399.
33. Ouattara B, Duplessis M, Girard CL. Optimization and validation of a reversed-phase high performance liquid chromatography method for the measurement of bovine liver methylmalonyl-coenzyme a mutase activity. *BMC Biochem*. 2013;14:25.
34. Chandler RJ, Venditti CP. Long-term rescue of a lethal murine model of methylmalonic acidemia using adeno-associated viral gene therapy. *Mol Ther*. 2010;18(1):11–16.
35. Hauser NS, Manoli I, Graf JC, Sloan J, Venditti CP. Variable dietary management of methylmalonic acidemia: metabolic and energetic correlations. *Am J Clin Nutr*. 2011;93(1):47–56.
36. Xu J, et al. Fibroblast growth factor 21 reverses hepatic steatosis, increases energy expenditure, and improves insulin sensitivity in diet-induced obese mice. *Diabetes*. 2009;58(1):250–259.
37. Fisher FM, Maratos-Flier E. Understanding the physiology of FGF21. *Annu Rev Physiol*. 2016;78:223–241.
38. Chandler RJ, et al. Vector design influences hepatic genotoxicity after adeno-associated virus gene therapy. *J Clin Invest*. 2015;125(2):870–880.
39. Umberger TS, et al. Novel sandwich immunoassays for the measurement of total and active FGF21. *Bioanalysis*. 2014;6(24):3283–3293.
40. Kruszka PS, Manoli I, Sloan JL, Kopp JB, Venditti CP. Renal growth in isolated methylmalonic acidemia. *Genet Med*. 2013;15(12):990–996.
41. Peters H, et al. A knock-out mouse model for methylmalonic aciduria resulting in neonatal lethality. *J Biol Chem*. 2003;278(52):52909–52913.
42. Peters HL, Pitt JJ, Wood LR, Hamilton NJ, Sarsero JP, Buck NE. Mouse models for methylmalonic aciduria. *PLoS One*. 2012;7(7):e40609.
43. Forny P, et al. Novel mouse models of methylmalonic aciduria recapitulate phenotypic traits with a genetic dosage effect. *J Biol Chem*. 2016;291(39):20563–20573.
44. An D, et al. Systemic messenger RNA therapy as a treatment for methylmalonic acidemia. *Cell Rep*. 2017;21(12):3548–3558.
45. Matsuishi T, Stumpf DA, Seliem M, Eguren LA, Chrislip K. Propionate mitochondrial toxicity in liver and skeletal muscle: acyl CoA levels. *Biochem Med Metab Biol*. 1991;45(2):244–253.
46. Walter JH, Thompson GN, Leonard JV, Bartlett K, Halliday D. Contribution of aminoacid catabolism to propionate production in methylmalonic acidaemia. *Lancet*. 1989;1(8650):1298–1299.
47. Imbard A, et al. Long-term liver disease in methylmalonic and propionic acidemias. *Mol Genet Metab*. 2018;123(4):433–440.
48. Ruppert T, et al. Molecular and biochemical alterations in tubular epithelial cells of patients with isolated methylmalonic aciduria. *Hum Mol Genet*. 2015;24(24):7049–7059.
49. Eid N, Ito Y, Horibe A, Otsuki Y. Ethanol-induced mitophagy in liver is associated with activation of the PINK1-Parkin pathway triggered by oxidative DNA damage. *Histol Histopathol*. 2016;31(10):1143–1159.
50. Ni HM, Williams JA, Jaeschke H, Ding WX. Zonated induction of autophagy and mitochondrial spheroids limits acetaminophen-induced necrosis in the liver. *Redox Biol*. 2013;1:427–432.
51. Wang AW, et al. TRAP-seq identifies cystine/glutamate antiporter as a driver of recovery from liver injury. *J Clin Invest*. 2018;128(6):2297–2309.

52. Hennig EE, et al. Extracellular matrix and cytochrome P450 gene expression can distinguish steatohepatitis from steatosis in mice. *J Cell Mol Med*. 2014;18(9):1762–1772.
53. Sahini N, Selvaraj S, Borlak J. Whole genome transcript profiling of drug induced steatosis in rats reveals a gene signature predictive of outcome. *PLoS One*. 2014;9(12):e114085.
54. Paz-Filho G, et al. Molecular pathways involved in the improvement of non-alcoholic fatty liver disease. *J Mol Endocrinol*. 2013;51(1):167–179.
55. Inagaki T, et al. Endocrine regulation of the fasting response by PPARalpha-mediated induction of fibroblast growth factor 21. *Cell Metab*. 2007;5(6):415–425.
56. Badman MK, Pissios P, Kennedy AR, Koukos G, Flier JS, Maratos-Flier E. Hepatic fibroblast growth factor 21 is regulated by PPARalpha and is a key mediator of hepatic lipid metabolism in ketotic states. *Cell Metab*. 2007;5(6):426–437.
57. Li Y, et al. Hepatic SIRT1 attenuates hepatic steatosis and controls energy balance in mice by inducing fibroblast growth factor 21. *Gastroenterology*. 2014;146(2):539–49.e7.
58. Banks AS, et al. SirT1 gain of function increases energy efficiency and prevents diabetes in mice. *Cell Metab*. 2008;8(4):333–341.
59. Purushotham A, Schug TT, Xu Q, Surapureddi S, Guo X, Li X. Hepatocyte-specific deletion of SIRT1 alters fatty acid metabolism and results in hepatic steatosis and inflammation. *Cell Metab*. 2009;9(4):327–338.
60. Kharitonenkov A, et al. FGF-21 as a novel metabolic regulator. *J Clin Invest*. 2005;115(6):1627–1635.
61. Badman MK, Koester A, Flier JS, Kharitonenkov A, Maratos-Flier E. Fibroblast growth factor 21-deficient mice demonstrate impaired adaptation to ketosis. *Endocrinology*. 2009;150(11):4931–4940.
62. Kharitonenkov A, et al. The metabolic state of diabetic monkeys is regulated by fibroblast growth factor-21. *Endocrinology*. 2007;148(2):774–781.
63. Kirmse B, Cabrerra-Luque J, Ayyub O, Cusmano K, Chapman K, Summar M. Plasma fibroblast growth factor-21 levels in patients with inborn errors of metabolism. *Mol Genet Metab Rep*. 2017;13:52–54.
64. Dushay J, et al. Increased fibroblast growth factor 21 in obesity and nonalcoholic fatty liver disease. *Gastroenterology*. 2010;139(2):456–463.
65. Suomalainen A, et al. FGF-21 as a biomarker for muscle-manifesting mitochondrial respiratory chain deficiencies: a diagnostic study. *Lancet Neurol*. 2011;10(9):806–818.
66. Lehtonen JM, et al. FGF21 is a biomarker for mitochondrial translation and mtDNA maintenance disorders. *Neurology*. 2016;87(22):2290–2299.
67. Reinehr T, Woelfle J, Wunsch R, Roth CL. Fibroblast growth factor 21 (FGF-21) and its relation to obesity, metabolic syndrome, and nonalcoholic fatty liver in children: a longitudinal analysis. *J Clin Endocrinol Metab*. 2012;97(6):2143–2150.
68. Molema F, Jacobs EH, Onkenhout W, Schoonderwoerd GC, Langendonk JG, Williams M. Fibroblast growth factor 21 as a biomarker for long-term complications in organic acidemias [published online ahead of print August 28, 2018]. *J Inherit Metab Dis*. https://doi.org/10.1007/s10545-018-0244-6.
69. Coate KC, et al. FGF21 is an exocrine pancreas secretagogue. *Cell Metab*. 2017;25(2):472–480.
70. Wang X, Wei W, Krzeszinski JY, Wang Y, Wan Y. A liver-bone endocrine relay by IGFBP1 promotes osteoclastogenesis and mediates FGF21-induced bone resorption. *Cell Metab*. 2015;22(5):811–824.
71. Wei W, et al. Fibroblast growth factor 21 promotes bone loss by potentiating the effects of peroxisome proliferator-activated receptor γ. *Proc Natl Acad Sci USA*. 2012;109(8):3143–3148.
72. Yun J, Finkel T. Mitohormesis. *Cell Metab*. 2014;19(5):757–766.
73. Owusu-Ansah E, Song W, Perrimon N. Muscle mitohormesis promotes longevity via systemic repression of insulin signaling. *Cell*. 2013;155(3):699–712.
74. Hine C, et al. Endogenous hydrogen sulfide production is essential for dietary restriction benefits. *Cell*. 2015;160(1-2):132–144.
75. Manoli I, Alesci S, Blackman MR, Su YA, Rennert OM, Chrousos GP. Mitochondria as key components of the stress response. *Trends Endocrinol Metab*. 2007;18(5):190–198.
76. Maratos-Flier E. Fatty liver and FGF21 physiology. *Exp Cell Res*. 2017;360(1):2–5.
77. Kharitonenkov A, DiMarchi R. Fibroblast growth factor 21 night watch: advances and uncertainties in the field. *J Intern Med*. 2017;281(3):233–246.
78. Ferrari M, et al. Hypoxia treatment reverses neurodegenerative disease in a mouse model of Leigh syndrome. *Proc Natl Acad Sci USA*. 2017;114(21):E4241–E4250.
79. Jain IH, et al. Hypoxia as a therapy for mitochondrial disease. *Science*. 2016;352(6281):54–61.
80. Ristow M. Unraveling the truth about antioxidants: mitohormesis explains ROS-induced health benefits. *Nat Med*. 2014;20(7):709–711.
81. Chandler RJ, et al. Adenoviral-mediated correction of methylmalonyl-CoA mutase deficiency in murine fibroblasts and human hepatocytes. *BMC Med Genet*. 2007;8:24.
82. Donoviel DB, Shield MA, Buskin JN, Haugen HS, Clegg CH, Hauschka SD. Analysis of muscle creatine kinase gene regulatory elements in skeletal and cardiac muscles of transgenic mice. *Mol Cell Biol*. 1996;16(4):1649–1658.
83. Lock M, et al. Rapid, simple, and versatile manufacturing of recombinant adeno-associated viral vectors at scale. *Hum Gene Ther*. 2010;21(10):1259–1271.